Received: 13 April 2022 | Revised: 23 August 2022 | Accepted: 24 August 2022

DOI: 10.1111/apha.13881

ACTA PHYSIOLOGICA

RESEARCH PAPER

Cholinergic signaling impairs cardiomyocyte cohesion

Sunil Yeruva | **Lars Körber** | **Matthias Hiermaier** | **Desalegn T. Egu** | **Ellen Kempf** | **Jens Waschke**

Chair of Vegetative Anatomy, Institute of Anatomy, Faculty of Medicine, Ludwig-Maximilian-University (LMU) Munich, Munich, Germany

Correspondence
Jens Waschke, Chair of Vegetative Anatomy, Institute of Anatomy, Faculty of Medicine, Ludwig-Maximilian-University (LMU) Munich, Pettenkoferstrasse 11, 80336 Munich, Germany.
Email: jens.waschke@med.uni-muenchen.de

Funding information
Deutsche Forschungsgemeinschaft, Grant/Award Number: WA2474/11-1; Fredrich-Baur-stifftung, Grant/Award Number: Reg.-Nr. 01/19

Abstract

Aim: Cardiac autonomic nervous system (ANS) dysregulation is a hallmark of several cardiovascular diseases. Adrenergic signaling enhanced cardiomyocyte cohesion via PKA-mediated plakoglobin phosphorylation at serine 665, referred to as positive adhesiotropy. This study investigated cholinergic regulation of cardiomyocyte cohesion using muscarinic receptor agonist carbachol (CCH).

Methods: Dissociation assays, Western blot analysis, immunostaining, atomic force microscopy (AFM), immunoprecipitation, transmission electron microscopy (TEM), triton assays, and siRNA knockdown of genes were performed in either HL-1 cells or plakoglobin (PG) wild type ($Jup^{+/+}$) and knockout ($Jup^{-/-}$) mice, which served as a model for arrhythmogenic cardiomyopathy.

Results: In HL-1 cells grown in norepinephrine (NE)-containing medium for baseline adrenergic stimulation, and murine cardiac slice cultures from $Jup^{+/+}$ and $Jup^{-/-}$ mice CCH treatment impaired cardiomyocyte cohesion. Immunostainings and AFM experiments revealed that CCH reduced desmoglein 2 (DSG2) localization and binding at cell borders. Furthermore, CCH reduced intercalated disc plaque thickness in both $Jup^{+/+}$ and $Jup^{-/-}$mice, evidenced by TEM analysis. Immunoprecipitation experiments in HL-1 cells revealed no changes in DSG2 interaction with desmoplakin (DP), plakophilin 2 (PKP2), PG, and desmin (DES) after CCH treatment. However, knockdown of any of the above proteins abolished CCH-mediated loss of cardiomyocyte cohesion. Furthermore, in HL-1 cells, CCH inhibited adrenergic-stimulated ERK phosphorylation but not PG phosphorylation at serine 665. In addition, CCH activated the AKT/GSK-3β axis in the presence of NE.

Conclusion: Our results demonstrate that cholinergic signaling antagonizes the positive effect of adrenergic signaling on cardiomyocyte cohesion and thus causes negative adhesiotropy independent of PG phosphorylation.

KEYWORDS

adrenergic signaling, cardiomyocyte cohesion, cholinergic signaling, desmoglein 2, desmoplakin, glycogen synthase kinase-3β

Sunil Yeruva and Lars Körber are equal first authors.

1 | INTRODUCTION

The autonomic nervous system (ANS), which comprises the sympathetic and parasympathetic nervous system (PNS), plays a vital role in the physiological and pathophysiological function of the heart.[1–3] The sympathetic nervous system (SNS) via β-adrenergic receptors (adrenergic signaling) increases heart rate, contractile forces, and conduction velocity. In contrast, PNS via muscarinic receptors (cholinergic signaling) has opposite effects. PNS acts through the vagus nerve, which carries the signal to the heart, where acetylcholine is released to stimulate cardiac muscarinic (M) receptors. The human body consists of five muscarinic (M) receptor subtypes (M1 - M5), of which four (M1-M4) are expressed in cardiac tissue. In addition, it was reported that PNS controls heart functions primarily via M2 and M3 receptors.[4–6]

Arrhythmogenic cardiomyopathy (AC), an arrhythmic heart disorder, is characterized by a mechanical and electrical communication deficiency among cardiomyocytes. The intercalated disc (ICD), a well-known functional unit of cardiomyocytes, harbors proteins that interact mechanically and electrically to maintain cardiomyocyte rigidity and synchrony.[7] Cardiac myocyte cohesive strength is necessary for strong mechanical coupling and is provided by desmosomes and adherens junctions (AJ) present in ICDs.[8] In cardiomyocytes, desmosomes are composed of desmoglein 2 (DSG2) and desmocollin 2 (DSC2), whereas AJs are composed of N-cadherin (N-CAD). Electrical coupling in cardiomyocytes is provided by the most abundantly expressed protein connexin 43 (Cx43),[8] which forms gap junctions (GJ) to provide the exchange of ions and other small molecules. It has been observed that GJ formation and function are regulated by desmosomal components in the ICDs.[8,9]

Previously, we provided the first evidence of β-adrenergic signaling to enhance cardiomyocyte cell cohesion via PKA-mediated phosphorylation of PG at serine 665, referred to as positive adhesiotropy.[10] Similarly, digitoxin, an inotropic agent, positively regulated cardiomyocyte cohesion.[11] As cardiac stimulation by the PNS is associated with reduced chronotropy and inotropy, and is known to act antagonistically to the SNS, we hypothesized that cardiomyocyte cohesion by the PNS could be regulated in an opposite manner. Therefore, in this study, we investigated the role of cholinergic signaling in cardiomyocyte cohesion. We show here for the first time that cholinergic signaling activation by carbachol, in both HL-1 cells and murine ventricular cardiac slices from wild-type and an AC murine model ($Jup^{-/-}$ mice), antagonizes the positive adhesiotropy of adrenergic signaling on cardiomyocyte cohesion and thus causes negative adhesiotropy, which is independent of PG phosphorylation.

2 | RESULTS

2.1 | Cholinergic signaling by carbachol (CCH) reduced cardiomyocyte cohesion

To investigate the effects of cholinergic signaling on cardiomyocyte cohesion, we utilized HL-1 cells (mouse atrial myocytes), which are extensively used as cardiomyocyte cell line,[12] as well as ex vivo murine cardiac slice cultures, and performed dispase-based dissociation assays to quantify cohesion. We first treated HL-1 cells with dosage of 10, 20, and 40 μM carbachol for 1 h and dissociation assay clearly showed a dose-dependent increase in the number of cell monolayer fragments due to loss of cell cohesion. Significant effects were seen at 40 μM CCH concentration (Figure 1A). Therefore, in all our further experiments, we used 40 μM CCH concentration. To explore whether the observed decrease in HL-1 cell cohesion exists in the intact cardiac tissue, we used a modified dispase assay in murine cardiac slices as described before.[10] Similar to HL-1 cells, we found that treating murine cardiac slices with CCH for 1 h led to a significant decrease in cell cohesion in both $Jup^{+/+}$ and $Jup^{-/-}$mice (Figure 1B). We next performed immunostainings in HL-1 cells to determine if the observed reduction in cell cohesion by CCH was paralleled by a change in DSG2 localization at the sites of cell–cell contacts. To explore this, we used N-CAD, an adherens junction protein, as a marker of cell–cell contacts and measured DSG2 localization in these regions as was done previously.[13] Immunostaining in HL-1 cells revealed a significant decrease in DSG2 at cell–cell contacts (Figure 1C and D), whereas triton assays performed in HL-1 cells to analyze changes in the cytoskeleton-bound fraction of the proteins DSG2, DP, PG, and β-catenin did not show any alteration (Supplementary Figure S1). These results demonstrated that decreased cardiomyocyte cell cohesion in response to cholinergic signaling was paralleled by a reduction of DSG2 at cell–cell contacts.

2.2 | CCH reduced DSG2-binding frequency in HL-1 cells

Since we observed a decrease in DSG2 localization at the membrane after CCH treatment, we further assessed the role of CCH in DSG2-binding efficiency and unbinding force. For this, we performed atomic force microscopy (AFM) using HL-1 cardiomyocytes as described before.[10] In this experiment, a cantilever with a DSG2 protein-coated tip approached the cells, where the DSG2 at the tip could eventually interact with the available DSG2, desmocollin (DSC) 2, or N-CAD, all of which are binding partners for DSG2[14] at the cell border and surface. The areas were chosen using a topography image of the cells,

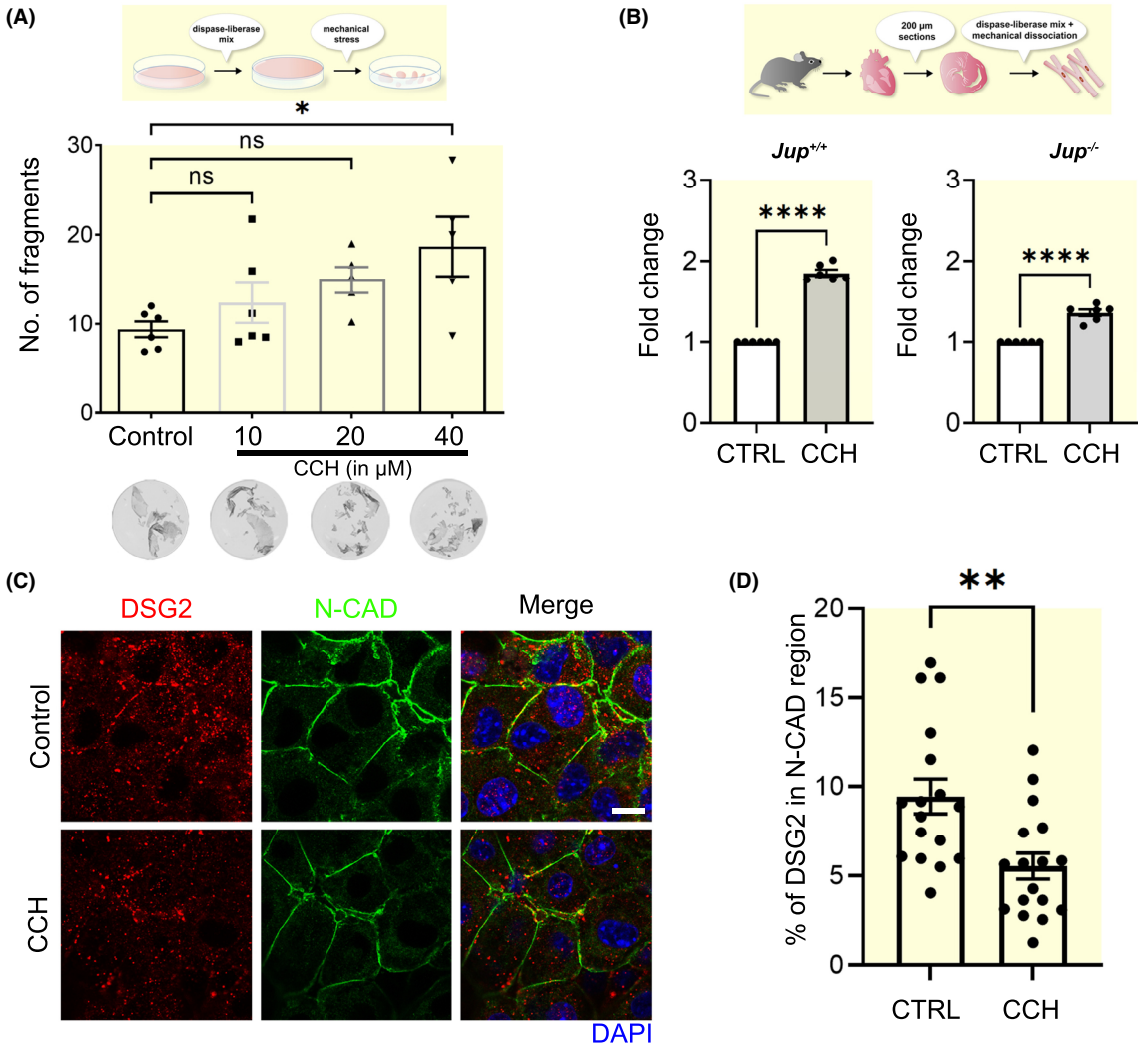

FIGURE 1 CCH impaired cardiomyocyte cohesion. (A) Dispase-based dissociation assay (cartoon illustrates the method) in HL-1 cardiomyocytes, with representative pictures of the wells, upon treatment with different doses of CCH for 1 h as mentioned respectively. *$p \leq 0.05$, one-way ANOVA with Holm-Šídák's multiple comparisons test, $N = 5$–6. (B) Dispase-based dissociation assay in murine cardiac slice cultures (cartoon illustrates the method) obtained from $Jup^{+/+}$ and $Jup^{-/-}$ mice incubated with control (CTRL) and 40 µM CCH for 1 h, ****$p \leq 0.0005$, Student's unpaired *t*-test, $N = 6$ per genotype. (C) Immunostaining in HL-1 cardiomyocytes for N-CAD and DSG2 showing a decrease of DSG2 at the cell–cell contacts after 1 h CCH treatment. White arrows indicate DSG2 localization at the cell membrane. Scale bar: 10 µm. (D) Quantification of colocalization of N-CAD and DSG2 in HL-1 cardiomyocytes, **$p \leq 0.05$, Student's unpaired *t*-test. Each data point represents data analyzed from one confocal image from $N = 3$–4 individual experiments. [Correction added on September 30, 2022 after first online publication. The figure 1 has been replaced in the article.]

acquired in the force-based quantitative imaging mode (Figure 2A). Upon CCH treatment, the binding frequency of DSG2 at both cell borders and cell surface significantly decreased (Figure 2B), whereas no changes were observed in terms of unbinding force (Supplementary Figure S2). In the control cell borders, a binding frequency of 43.2 ± 5.8% was observed, which upon CCH treatment reduced to 34 ± 6. In addition, we measured a binding frequency of 46.5 ± 2.8% at the cell surface, which reduced to 32.6 ± 4.8 upon CCH treatment. These data indicate that CCH reduced DSG2 adhesion by reducing the binding frequency, which correlated with the observed reduction in intercellular cohesion and DSG2 localization at the cell–cell contacts in HL-1 cardiomyocytes.

2.3 | CCH reduced plaque thickness in the cardiomyocyte ICD

Since we observed that CCH reduced DSG2 localization and binding at cell borders, we further investigated whether CCH causes any alterations in the ultrastructure of ICD. We performed transmission electron microscopy (TEM) in CCH-treated murine cardiac slices from both $Jup^{+/+}$ and

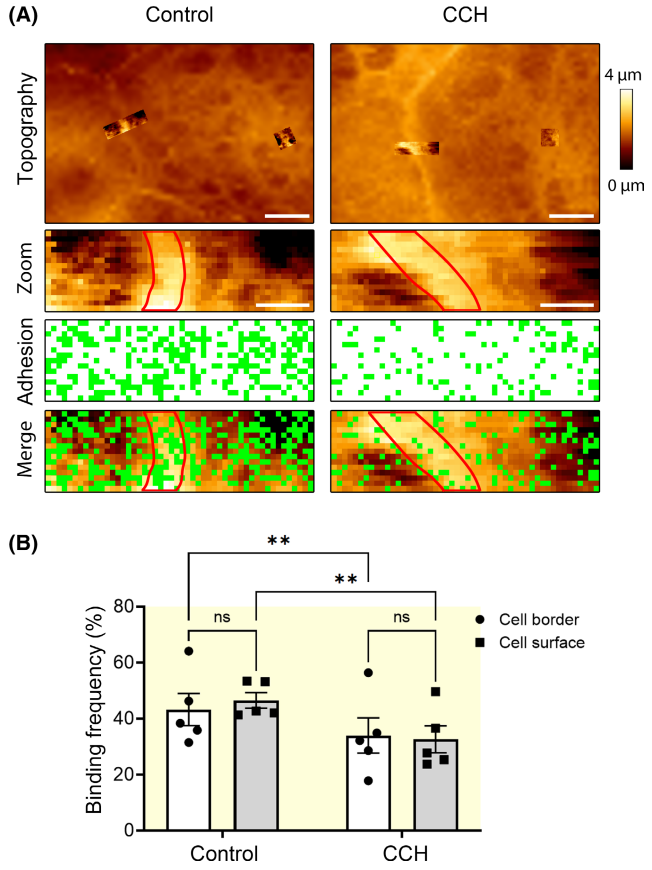

FIGURE 2 CCH treatment of HL-1 cells reduced DSG2-binding frequency. (A) Topography images obtained during AFM measurements on HL-1 cardiomyocytes before and after 1 h CCH treatment at cell borders and cell surfaces with DSG2 coated tips. Green dots in topography images indicate binding events; red lines indicate cell borders. Topography images are 1.5 µm × 5 µm. (B) Quantification of DSG2-binding frequency expressed in percentage. Each data point represents 1500 curves analyzed across two areas (1.5 µm × 5 µm). *$p \leq 0.05$, two-way repeated measure ANOVA with Tukey's post-hoc test was performed. $N = 5$.

Jup$^{-/-}$ mice and measured area composita lengths and plaque thickness, as described before.[15] TEM revealed that CCH reduced intercalated disc plaque thickness in both *Jup*$^{+/+}$ and *Jup*$^{-/-}$mice (Figure 3A and C), whereas no changes were observed in area composita lengths (Figure 3A and D). In *Jup*$^{+/+}$ mice, we measured a plaque thickness of 102.5 ± 2.7 nm, which was reduced to 93.6 ± 2.5, whereas in *Jup*$^{-/-}$ mice, we observed a plaque thickness of 84.7 ± 2.1 nm, which reduced to 72 ± 2.6 nm upon CCH treatment.

2.4 | CCH reduced desmoplakin in the cardiomyocyte ICD

Since plaque thickness was decreased in the ICD after CCH treatment, we further assessed the localization of desmosomal proteins in the ICD. To analyze this, we performed immunostaining utilizing wild type (*wt*) mice and measure the intensities of DSG2, DP, PG, and PKP2 using wheat germ agglutinin as a marker for ICD (Figure 4). Quantitative analysis revealed a decrease in DP immunostaining intensity in the ICD (Figure 4B) whereas staining for PG and PKP2 did not alter (Figure 4C and D). However, a decrease in DSG2 immunostaining intensity was also observed but was not statistically significant (Figure 4A).

2.5 | CCH-mediated reduction in cell cohesion is dependent on intact desmosome composition

Since we observed changes in plaque thickness and reduction of DP in the ICD, we investigated which desmosomal component is necessary for CCH-mediated cardiomyocyte cohesion regulation. For this, we utilized HL-1 cells, where we used siRNA to knockdown either desmoglein 2 (Dsg2), desmoplakin (Dp), plakoglobin (Jup) or plakophilin 2 (Pkp2) mRNA transcripts and performed dissociation assays. Dissociation assays revealed that depletion of any of the above genes did not cause significant changes in cohesion except for Dp where we saw an increase in number of fragments but was not statistically significant (Supplementary Figure S3A). Whereas depletion of any of the above genes abrogated CCH-mediated reduction in HL-1 cell cohesion, demonstrating that the presence of all desmosomal components is necessary for the loss of cardiomyocyte cohesion in response to CCH (Figure 5A and B; Supplementary Figure S3B).

Thus, by immunoprecipitation, we further investigated whether CCH causes a change in the interaction of desmosomal components. We pulled down DSG2 from HL-1 cells treated with and without CCH. However, co-immunoprecipitation of DP, PG, PKP2, and desmin (DES) did not reveal any reduction in their interaction with DSG2 (Figure 4C and Supplementary Figure S3C).

2.6 | CCH reduced Forskolin-Rolipram (FR)-mediated increase in cardiomyocyte cohesion

We have previously shown that adrenergic signaling enhances cardiomyocyte cohesion. Since the PNS antagonizes the SNS effects in the heart, we further investigated if similar effects occur in cell cohesion. We performed dissociation assays in both HL-1 and *wt* murine cardiac slice cultures after incubation with a combination of CCH and FR. For this set of experiments, HL-1 cells were grown without a norepinephrine-containing medium to avoid the basal adrenergic signal activation. Dissociation assays revealed that

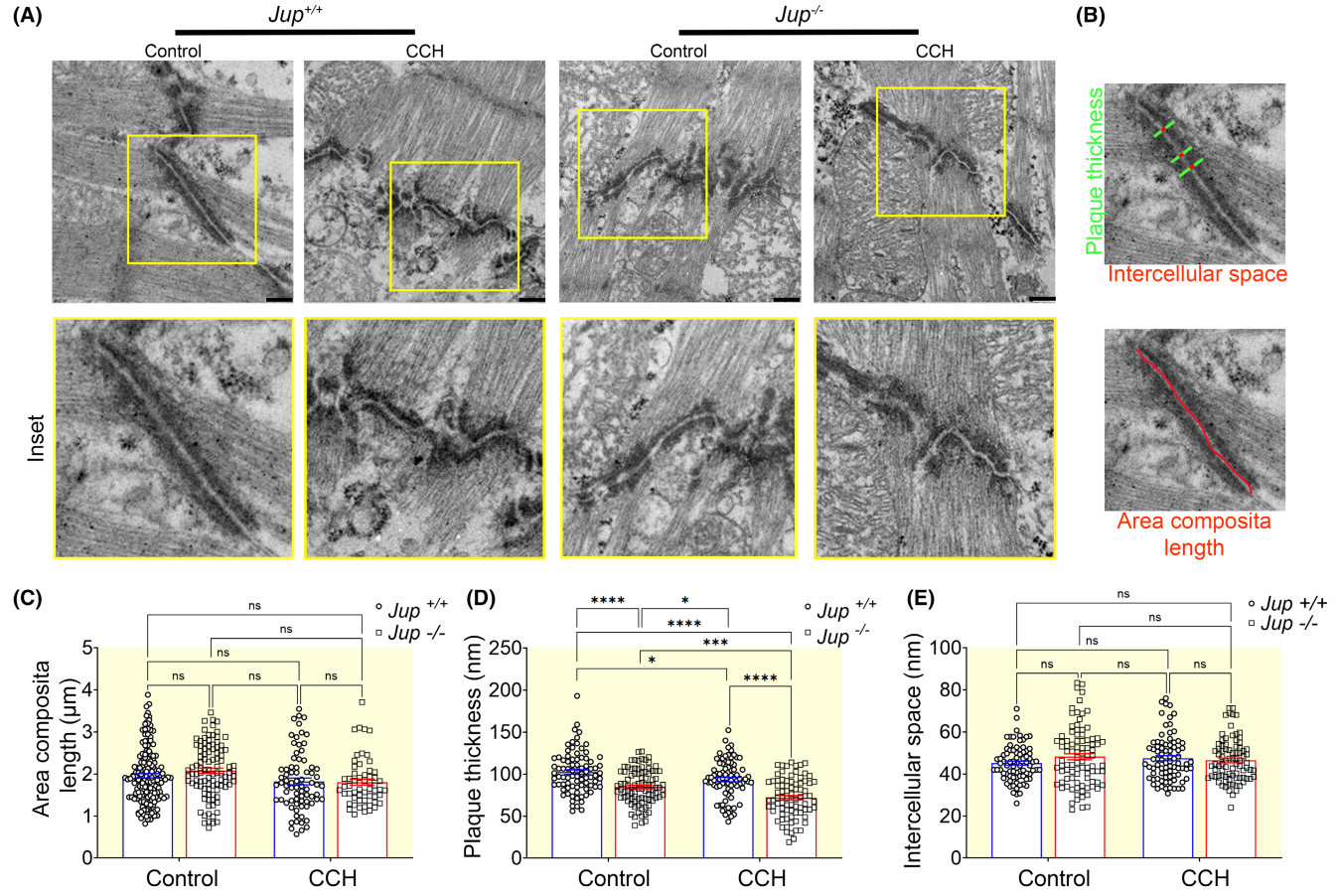

FIGURE 3 CCH-mediated ultrastructural changes in the ICDs of murine cardiomyocytes. (A) Transmission electron microscopy was performed from cardiac slices derived from hearts of 12-week-old $Jup^{+/+}$ and $Jup^{-/-}$ mice incubated with and without 40 μM CCH for 1 h and representative images were displayed. Scale bar: 250 nm. $N = 3$ mice per condition. Yellow squares were drawn, and insets were enlarged, as shown in the lower panel. (B) Exemplar images of how the analysis of junctional plaque thickness and area composita lengths were obtained (as explained in methods), (C, D, and E) bar graphs of plaque thickness, area composita lengths, and intercellular space measured from panel A. Each dot corresponds to one ICD. $^{*}p < 0.05$, $^{***}p < 0.0005$ $^{****}p < 0.00005$. $N = 3$ mice per genotype. Two-way repeated measure ANOVA with Tukey's post-hoc test was performed.

both in HL-1 cells and *wt* murine cardiac slices, CCH reduced FR-mediated cardiomyocyte cohesion (Figure 6A and B). Since we described that FR-mediated increase in cardiomyocyte cohesion requires either PKA-mediated phosphorylation of PG at serine 665 or ERK1 activation,[10,13,15] we next performed triton assays to find out if CCH reduced effects of FR by regulating these pathways. Triton assays in HL-1 cells revealed that CCH inhibits FR-mediated activation of ERK1 but not of ERK2 and also did not enhance PG phosphorylation at serine 665 (Figure 6C–E).

2.7 | PI3kinase(PI3K)-AKT-GSK-3β axis was involved in CCH-mediated loss of cardiomyocyte cohesion

Cholinergic signaling is known to activate the PI3K-AKT axis.[16,17] On the other hand, GSK-3β, a downstream target of AKT, was shown to be important in DP localization to the cell borders and desmosome formation.[18] Therefore, we questioned whether the observed reduction in DSG2 at the cell–cell contact could be regulated via this pathway. Dissociation assays performed in HL-1 cells treated with CCH in the presence and absence of Wortmannin, a PI3K/AKT pathway inhibitor, revealed that under constitutive adrenergic activation (presence of norepinephrine in the medium), Wortmannin abrogated CCH-mediated reduction of cardiomyocyte cohesion (Figure 7A). CCH caused an increase in GSK-3β phosphorylation at serine 9 (Figure 7B and C) and a reduction in the DP and DSG2 colocalization at cell–cell contacts (Figure 7D and E), which was abolished in the presence of Wortamannin, indicating that the PI3K-AKT-GSK-3β signaling axis is engaged in the negative regulation of cholinergic cardiomyocyte cohesion.

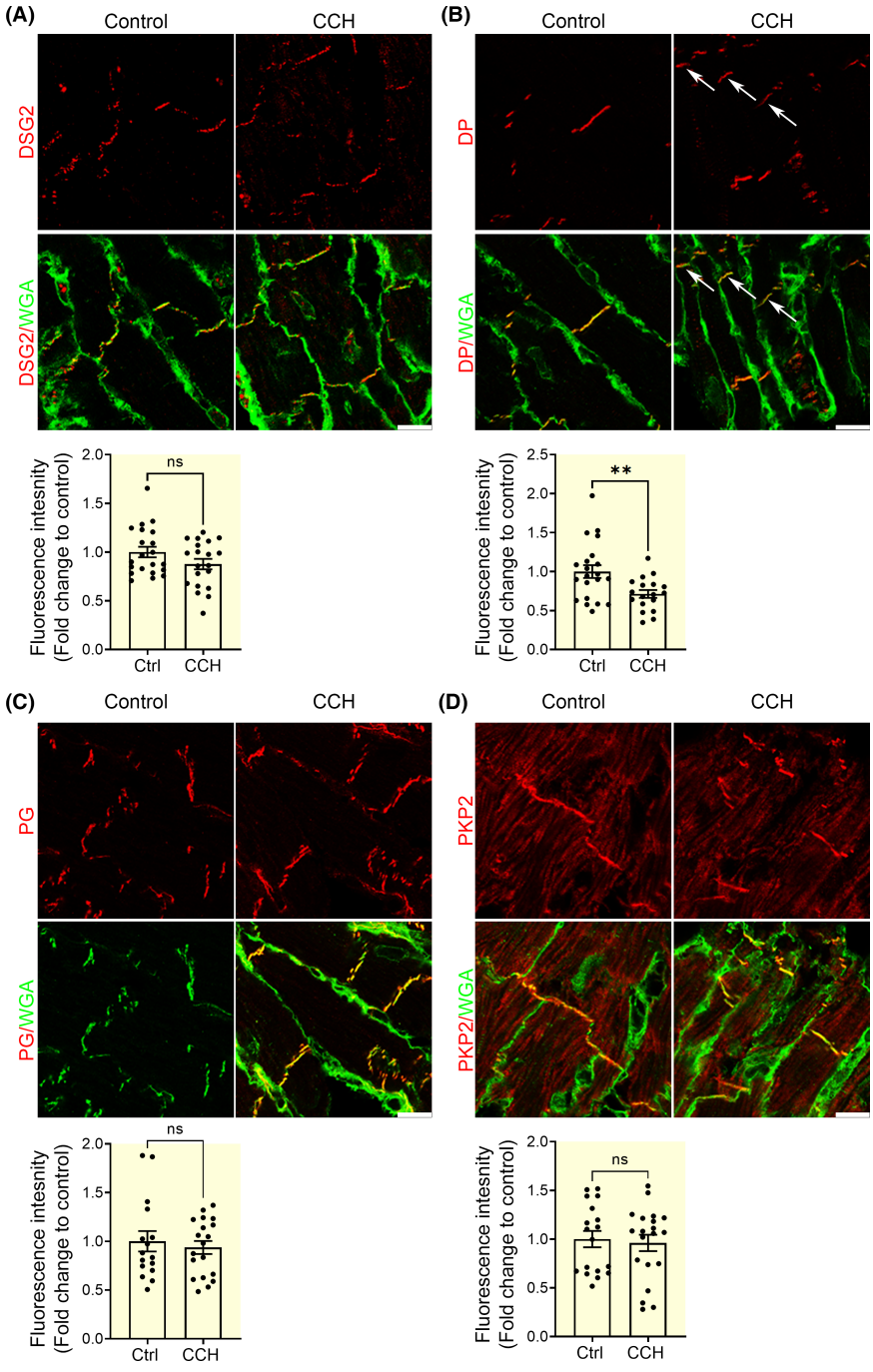

FIGURE 4 CCH-mediated changes of desmosomal proteins in the ICDs of murine cardiomyocytes. Immunostaining of desmosomal proteins (A) DSG2, (B) DP, (C) PG, and (D) PKP2 was performed from cardiac slices derived from hearts of 12-week-old *wt* mice incubated with and without 40 μM CCH for 1 h and representative images were displayed. Arrows indicate a decrease in fluorescence intensity in DP after CCH treatment. Scale bar: 10 μm. $N = 3$ mice per condition. Bar graphs represents fold change in fluorescence intensities of proteins measured in the ICD. Each dot corresponds to fluorescence intensities measured in one image, a minimum of three images per N were obtained. $^{*}p < 0.05$. Student *t*-test with Welch's correction was performed.

2.8 | CCH-mediated reduction of DSG2 interaction requires PI3K

Since the above experiments with Wortmannin revealed that CCH required PI3K-AKT-GSK-3β signaling axis, we further investigated whether the observed decrease in DSG2-binding frequency after CCH treatment was also dependent on the same signaling mechanism. Therefore, we performed AFM experiments in HL-1 cells treated with CCH in the presence of Wortmannin. DSG2-binding frequency was unaltered by CCH in the presence of Wortamannin (Figure 8), revealing that the observed decrease in DSG2 interaction by CCH required the PI3K-AKT-GSK-3β signaling axis.

3 | DISCUSSION

The ANS, which consists of SNS and PNS, is critical to the proper function of the heart. Alterations in the SNS and PNS could eventually lead to cardiac disorders such as congestive heart failure, sudden cardiac death, and myocardial ischemia.[19,20] Therefore, in the quest to understand the role of ANS in cardiomyocyte cohesion, we

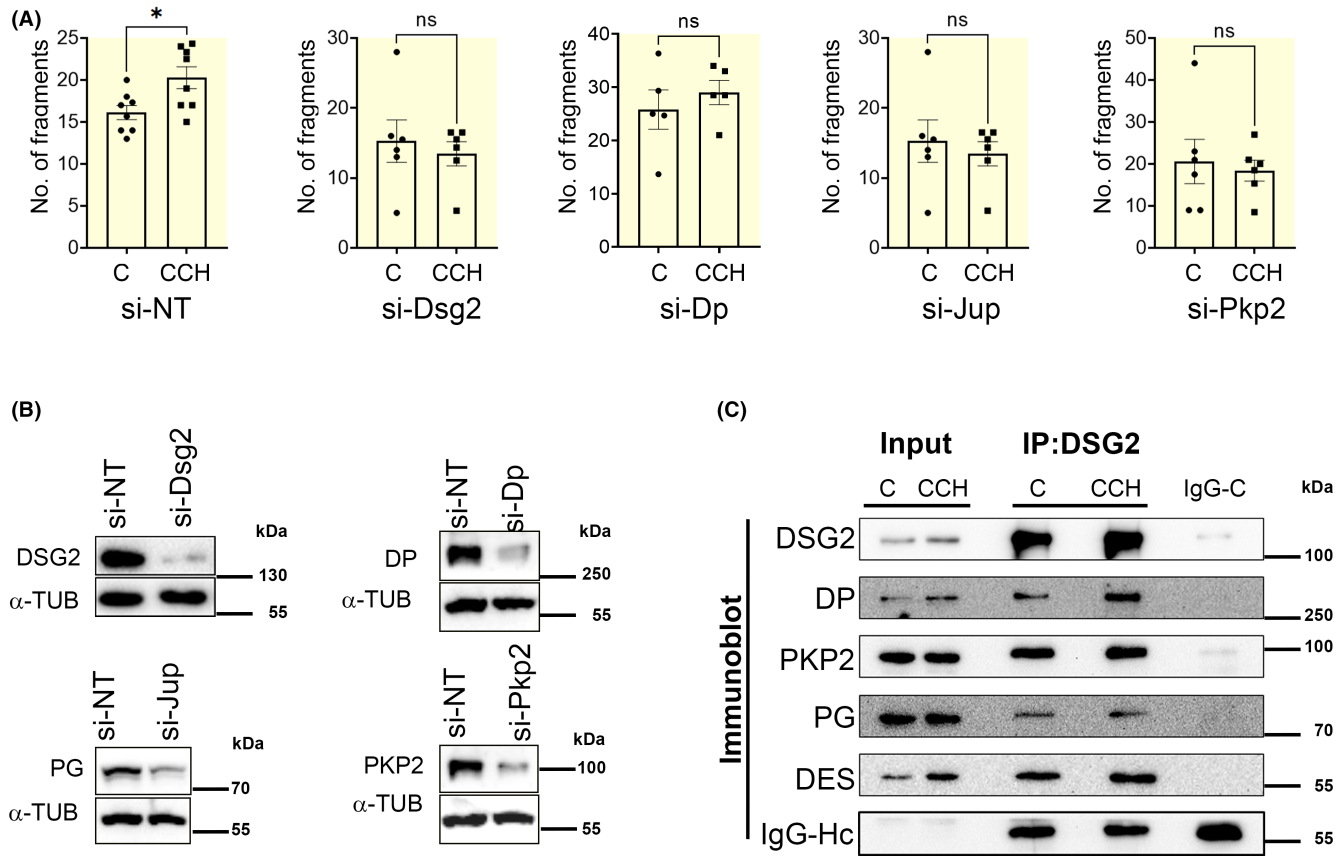

FIGURE 5 CCH-mediated inhibition of cardiomyocyte cohesion required all desmosomal components. (A) Dispase-based dissociation assay in HL-1 cardiomyocytes after siRNA-mediated knockdown of Dsg2, Dp, Jup, Pkp2 and non-target (NT) control knockdown. Student's unpaired *t*-test, $N = 4–9$. (B) Representative Western blot confirmation of siRNA-mediated knockdown efficiency for DSG2, DP, PG, and PKP2, α-tubulin (α-TUB) served as an internal loading control, $N = 4–9$. (C) Representative Western blots for immunoprecipitation of DSG2, co-immunoprecipitation of DP, PKP2, PG and DES, IgG heavy chain (IgG-Hc) served as loading control for immunoprecipitated samples, $N = 3–4$. C mean control.

have previously established that adrenergic signaling via PKA-mediated PG phosphorylation at serine 665 in ERK1/2-dependent manner enhanced cardiomyocyte cohesion and termed this phenomenon as positive adhesiotropy.[10,13,15,21] In this study, we further explored the role of cholinergic signaling in cardiomyocyte cohesion. We showed that cholinergic signaling antagonized the positive effect of adrenergic signaling on cardiomyocyte cohesion and thus caused negative adhesiotropy in a process independent of Pg phosphorylation.

HL-1 cells and murine cardiac slices from wild type mice treated with CCH showed a significant decrease in cardiomyocyte cohesion. In addition, in HL-1 cells CCH reduced the presence of DSG2 at cell–cell contacts. It has to be noted that HL-1 cells do not represent a mature cardiomyocyte, but they are the best cell type available to study cell cohesion since they form monolayers of the required surface area and reflect the results from slice culture models.[13] Similarly, in this study, dissociation assays performed in murine cardiac slices also resulted in the reduction of cardiomyocyte cohesion after CCH treatment, further confirming that the observed reduction of cell cohesion by CCH in HL-1 cells was not cell line dependent.

So far, the role of cholinergic signaling in cellular cohesion is limited to keratinocytes only, where cholinergic signaling was shown to stabilize desmosomal adhesion by enhancing the level of expression of both DSG 1 and DSG 3.[22,23] However, the role of cholinergic signaling neither in DSG2-mediated cell cohesion nor in cardiomyocyte cohesion was pursued. The observed cholinergic signaling effects of cardiomyocyte cohesion show the opposite of what was reported in keratinocytes which is in line with other signaling pathways with different outcomes in cardiomyocytes compared with epithelial cells.[21] For example, ERK1/2 activation in response to pemphigus autoantibodies caused a reduction in desmosomal adhesion in keratinocytes, whereas, in cardiomyocytes, the activation of ERK1/2 by adrenergic mediators enhanced cardiomyocyte cohesion.[21]

AFM experiments performed on live HL-1 cells revealed a decrease in DSG2-binding efficiency upon CCH treatment. Reduction in DSG2-binding efficiency was

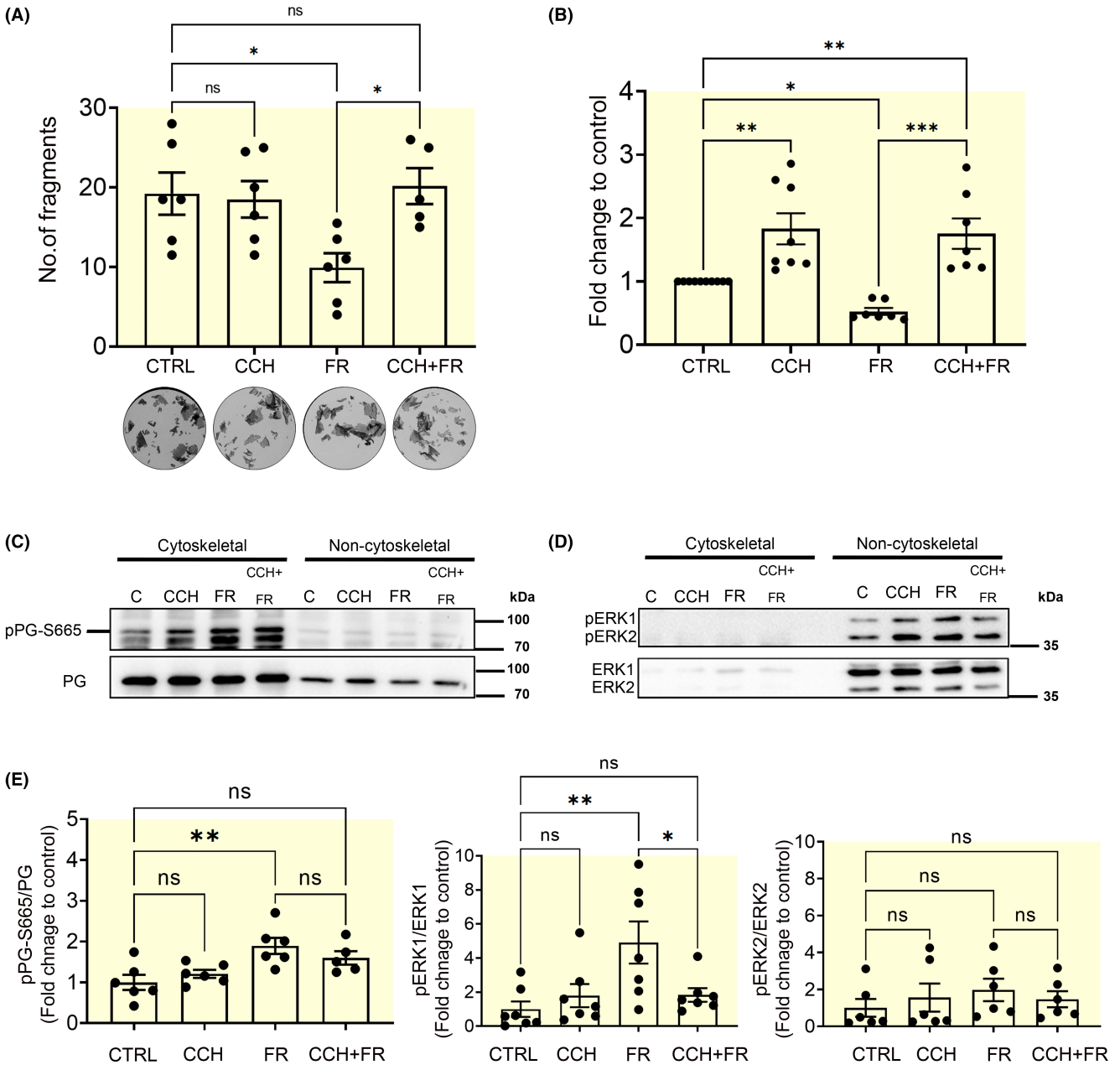

FIGURE 6 CCH reduced FR-mediated increase in cardiomyocyte cohesion. (A) Dispase-based dissociation assay in HL-1 cardiomyocytes treated with control, CCH, FR, and CCH + FR for 1 h, with representative pictures of the wells displayed at the bottom of the bar graph, $*p \leq 0.05$, one-way ANOVA with Holm-Šídák's multiple comparisons test, $N = 6$. (B) Dispase-based dissociation assay in murine cardiac slice cultures obtained from *wt* mice incubated with respective mediators for 1 h, $****p \leq 0.0005$, one-way ANOVA with Holm-Šídák's multiple comparisons test $N = 8$. (C and D) Representative Triton assay blots for protein expression of phospho-serine665 of PG (pPG-S665), pERK1 and pERK2, and their respective total proteins in HL-1 cells after treatment with mediators mentioned in the blot, $N = 6$–7. (E) Quantification of Western blots from C and D $*p \leq 0.05$, one-way ANOVA with Holm-Šídák's multiple comparisons test. C and CTRL mean 'control'.

observed both at the cell borders and cell surface. Since we observed a reduction of DSG2 at cell–cell contacts upon CCH treatment, a decrease in DSG2-binding efficiency may result from the obliteration of DSG2 molecules at cell junctions. Since previous studies performed in the field of pemphigus and intestinal epithelial cells identified the presence of extradesmosomal desmogleins,[24] the data indicate that similar to epithelial cells, extradesmosomal DSG2 is present in HL-1 cells and is also affected by cholinergic signaling.

Further in this study, we utilized a murine model of AC, *Jup* knockout mice, which was well characterized for the presence of fibrosis, arrhythmia, and altered desmosomal regulation in our previous studies.[10,11,13,15]

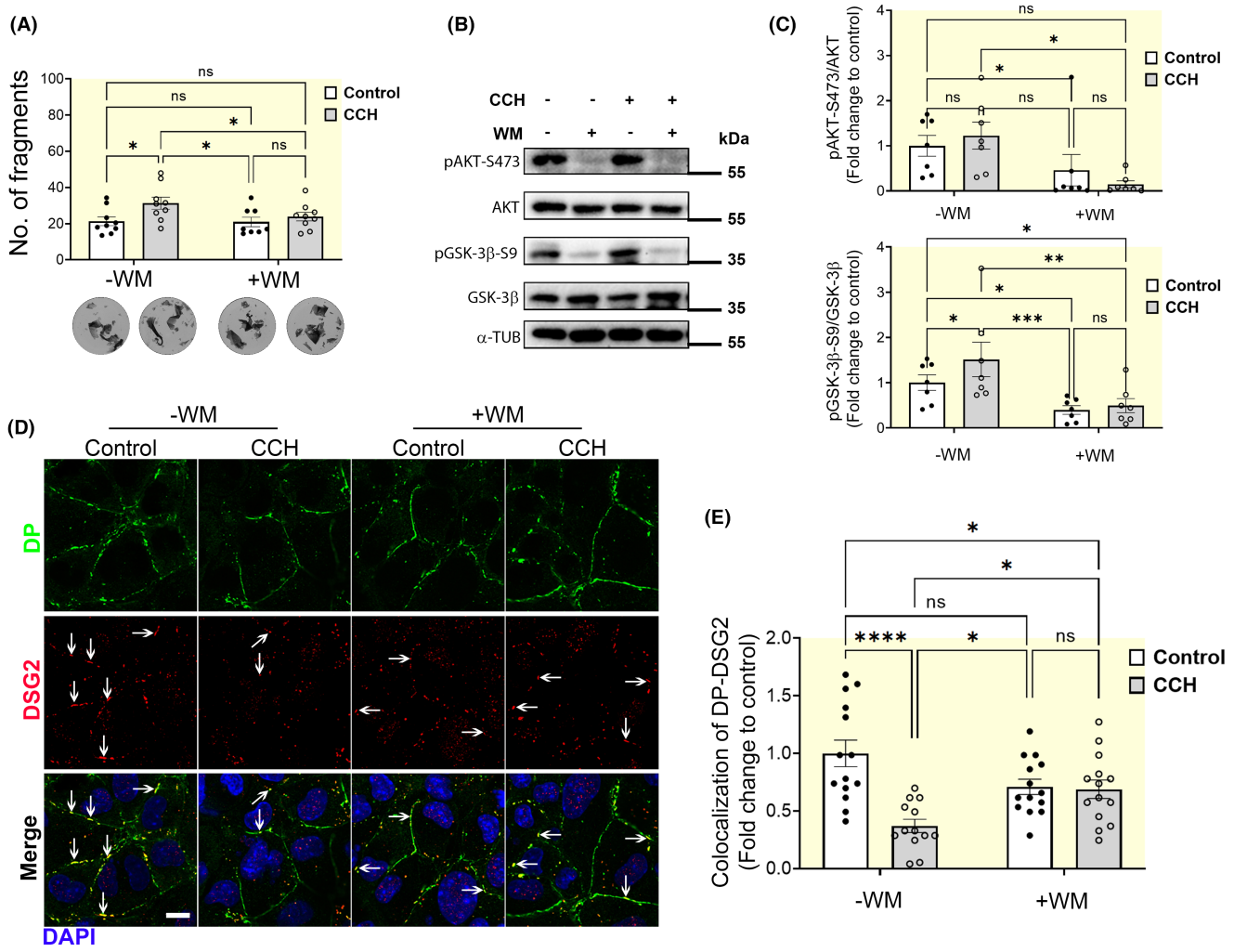

FIGURE 7 CCH impaired DP-DSG2 reduction at cell borders via PI3K-AKT-GSK-3β signaling. (A) Dispase-based dissociation assay in HL-1 cardiomyocytes treated with control, CCH, Wortmannin (WM) and CCH + WM for 1 h. HL-1 cells were incubated 30 min prior to the addition of CCH with WM. Representative pictures of the wells displayed at the bottom of the bar graph, $*p \leq 0.05$, one-way ANOVA with Holm-Šídák's multiple comparisons test, $N = 9–10$. (B) Representative Western blot showing protein expression of phospho-serine 473 of AKT (pAKTS473) and total AKT, phosphor-serine 9 of GSK-3β (pGSK-3βS9), and total GSK-3β in HL-1 cells treated as in a with respective mediators. $N = 6$. (C) Quantification of Western blot from b $*p \leq 0.05$, one-way ANOVA with Holm-Šídák's multiple comparisons test. (D). Immunostaining in HL-1 cardiomyocytes for DP and DSG2 showing a decrease in the colocalisation of DP-DSG2 at the cell–cell contacts after 1 h CCH treatment in the presence or absence of WM. White arrows indicate DP-DSG2 colocalization at the cell membrane. Scale bar: 10 μm. (E) Quantification of DP-DSG2 at the cell–cell contacts after 1 h CCH treatment in the presence or absence of WM in HL-1 cardiomyocytes, $**p \leq 0.05$, one-way ANOVA with Holm-Šídák's multiple comparisons test. Each data point represents data analyzed from one confocal image from $N = 3–4$ individual experiments.

Adrenergic signaling-mediated cardiomyocyte cohesion was abrogated entirely in *Jup*$^{-/-}$ mice,[10,13,15] and therefore we also studied the role of cholinergic signaling in these mice. Surprisingly, CCH effectively reduced *Jup*$^{-/-}$mice cardiomyocyte cohesion, suggesting alternative pathways for cholinergic signaling-mediated cardiomyocyte cohesion independent from PG. Since we observed a reduction in DSG2 localization and binding efficiency at the cell border of HL-1 cells, we anticipated ultrastructural changes at the ICD of cardiomyocytes; as in a previous study, we found out that adrenergic signaling enhanced area composita lengths and plaque thickness in *Jup*$^{+/+}$ mice, whereas these changes were completely absent in *Jup*$^{-/-}$ mice.[15] TEM analysis performed in the cardiac slices of *Jup*$^{+/+}$ *and Jup*$^{-/-}$ mice treated with and without CCH revealed no changes in the area composita lengths. Whereas, we found a significant decrease in the plaque thickness upon CCH treatment of cardiac slices from both *Jup*$^{+/+}$ *and Jup*$^{-/-}$ mice. Since the desmosomal plaque contains the proteins DP, PG, and PKP2, we further asked whether the observed changes in plaque thickness could be due to changes in the amount of these proteins in the ICD and

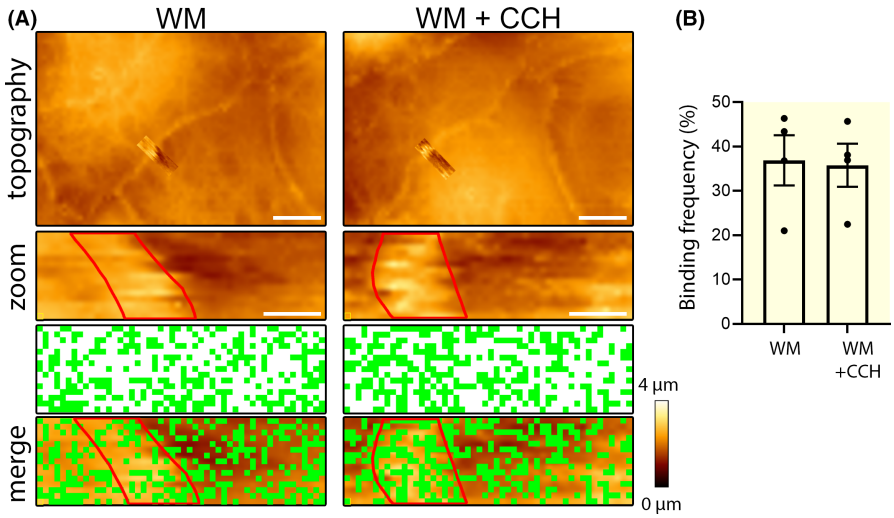

FIGURE 8 Inhibition of PI3K-AKT-GSK-3β signaling ameliorated CCH-mediated reduction of DSG2 binding frequency in HL-1 cells. (A) Topography images obtained during AFM measurements on HL-1 cardiomyocytes at cell borders with DSG2 coated tips after preincubating with Wortmannin for 30 min and CCH for 1 h. Green dots in topography images indicate binding events; red lines indicate cell borders. Topography images are 1.5 µm × 5 µm. (B) Quantification of DSG2 binding frequency expressed in percentage. Each data point represents 1500 curves analyzed across two areas (1.5 µm × 5 µm). *$p \leq 0.05$, Student *t*-test with Welch's correction was performed. $N = 4$.

performed immunostaining in *wt* mice cardiac slices. We found a decrease in the fluorescence intensity of DP after CCH treatment. Since it' is very well established that the inner dense plaque mainly consists of DP, our results indicate that the reduction in plaque thickness after CCH treatment could result from decreased DP at the ICD.

Further, in order to study whether other plaque proteins are required for cholinergic effects on desmosomal adhesion, we switched to HL-1 cells to knockdown the genes encoding for the desmosomal components. siRNA knockdowns experiments clearly indicated that besides DSG2, all desmosomal plaque components PG, DP, and PKP2 are necessary for cholinergic regulation of cell cohesion, at least in HL-1 cells. However, co-immunoprecipitation revealed no alterations in the desmosomal protein interactions in response to cholinergic signaling. This is in line to previous observations on adrenergic signaling,[15] indicating that for signaling-mediated fine-tuning of adhesion an intact composition of desmosomal contacts is required. However, in intact cardiac tissue, PG was not required for the negative effects of cholinergic signaling on cardiomyocyte cohesion, suggesting that PG is not a direct target. Moreover, compensatory mechanisms may be present in intact hearts that are ineffective under conditions of siRNA-mediated depletion of PG in cultured cells where junctions are immature compared with proper intercalated discs.

As both the SNS and PNS antagonize each other in terms of the physiological functions of the heart, we next investigated whether cholinergic signaling antagonizes the adrenergic positive adhesiotropy. In fact, it is very well established that cholinergic signaling acts by inhibiting adrenergic cAMP production.[25] Dissociation assay experiments performed using the combination of CCH and FR in HL-1 cells, and wild type murine cardiac slices revealed that cholinergic signaling inhibits adrenergic positive adhesiotropy. Furthermore, CCH significantly reduced FR-mediated ERK1 phosphorylation, whereas phosphorylation of PG at serine 665 was unaltered. These data suggest that cholinergic signaling does not completely blunt adrenergic signaling but instead interferes with some signaling pathways downstream of cAMP and not with PKA-mediated PG phosphorylation, which is required for positive adhesiotropy.

In the cardiomyocytes, cholinergic signaling is known to engage other signaling pathways such as PI3K/AKT, cGMP, PKG, and Ca/Calmodulin-dependent protein kinase II.[16,17,26] In mouse or zebrafish brain, in vivo administration of agents which increase cholinergic stimulation or block NMDA receptors led to an increase in the inhibitory phosphorylation site of GSK-3β at serine 9.[27–29] The desmosomal protein DP was shown to act as a scaffold for GSK-3β in cardiomyocytes. Moreover, this association was attenuated in AC patients with a mutation in the methylation site R2834 of DP.[18] In the same study, GSK-3β-mediated processive phosphorylation of the DP C-tail served as a switch to regulate the dynamic association of DP and intermediate filaments (IF) to facilitate DP trafficking and thereby formation of desmosomes. Based on this, we speculated that cholinergic signaling via the PI3K/AKT-mediated GSK-3-β inhibition would diminish DP association with IF. Indeed, dissociation assays performed in HL-1 cells revealed that CCH had no effect on cardiomyocyte cohesion in the presence of

PI3K inhibitor Wortmannin. In line with this, phosphorylation of GSK-3β at serine 9 was observed upon CCH treatment, and the decrease in DP-DSG2 colocalization at cell borders was abolished after PI3K inhibition. Since, a decrease in DSG2 interaction after CCH treatment was observed in AFM experiments performed on HL-1 cells, we further evaluated the possible role of PI3K-AKT-GSK-3β signaling axis in the above. In the presence of Wortmannin, CCH did not reduce DSG2 binding at the cell borders further revealing that PI3K-AKT-GSK-3β signaling axis is important for CCH-mediated reduction in DSG2 binding.

In conclusion, our results demonstrate that cholinergic signaling reduces cardiomyocyte cohesion under normal physiological and pathophysiological conditions as in PG-deficient mice in a process involving the PI3K-AKT-GSK-3β signaling axis (Figure 9), which we define as "negative adhesiotropy." Together with already available data that autoantibodies against muscarinic receptors exist in myocarditis and dilated cardiomyopathy patients which lead to the activation of muscarinic receptors and its downstream signaling pathways,[30–32] we speculate that cholinergic signaling may cause further reduction in mechanical strengths of cardiomyocyte cohesion in both desmosomal gene mutations carrying and non-carrying AC patients. Therefore, further studies focusing on which muscarinic receptors are involved in cholinergic signaling to regulate cardiomyocyte cohesion may lead to future therapeutics targeting muscarinic receptors in AC patients.

4 | MATERIALS AND METHODS

All the material submitted conform with good publishing practice in physiology according to the Acta Physiologica guidelines.

4.1 | Cell culture

As explained previously, the murine atrial cardiac myocyte cell line HL-1 was maintained.[13] In brief, cells were grown in Claycomb medium (#51800C) supplemented with 10% fetal bovine serum (#F2442), 100 µmol/L norepinephrine, 100 µg ml^{-1} penicillin/streptomycin, and 2 mmol L^{-1} L-glutamine at 37°C, 5% CO_2 and 100% humidity as described previously. All cell culture reagents were purchased from Sigma-Aldrich, Munich, Germany. After seeding for experiments, cells were incubated in Claycomb medium either containing norepinephrine (as a basal adrenergic stimulation) or without for the experiments where we used the combination of FR.

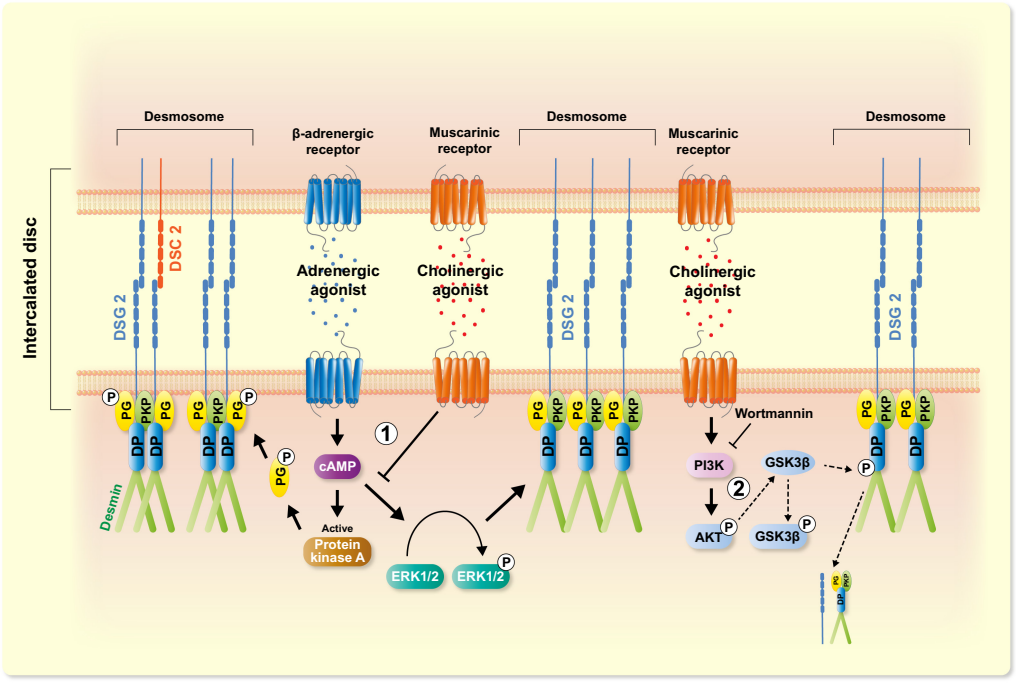

FIGURE 9 Cholinergic signaling impairs cardiomyocyte cohesion. Cholinergic signaling impairs cardiomyocyte cohesion by (1) reducing adrenergic signaling-mediated positive adhesiotropy via inhibiting ERK1/2 activation and thereby arresting the moment of DSG2 into the cell membrane and (2) activating PI3K-AKT-mediated phosphorylation of GSK-3β at serine 9 that leads to the inhibition of DP phosphorylation by GSK-3β, which in turn results in the disruption of DP-DSG2 interaction and thereby less DSG2 at the cell borders. However, in the presence of Wortmannin, cholinergic signaling could not impair cardiomyocyte cohesion.

4.2 | Arrhythmogenic mouse model and cardiac slice culture

Animal handling, breeding, and sacrifice were performed under approval of regulations by the regional government Upper Bavaria (Gz. ROB-55.2-2532.Vet_02–19-172). Plakoglobin (PG)-deficient mice ($Jup^{-/-}$) were generated and characterized as described previously.[10,11,13,15] In brief, mice with loxP sites flanking exon 1 of the junctional plakoglobin gene (*Jup*) on both alleles ($Jup^{tm1.1Glr}$/J mice, the Jackson Laboratory, Bar Harbor, USA) were bred with mice heterozygous for loxP sites in *Jup* with an expression of the recombinase Cre under the control of cardiac-specific alpha myosin heavy chain promoter (*Myh6*), which were generated by crossing with B6.FVB-Tg(Myh6-cre)2182Mds/J mice (The Jackson Laboratory). Twelve-week-old age and sex-matched littermates of $Jup^{+/+}$ and $Jup^{-/-}$ mice[10] were used for experiments. Murine slice cultures were obtained as described before.[10,11,13,15] In brief, mice were sacrificed by cervical dislocation, hearts were immediately placed in pre-cooled oxygenated cardiac slicing buffer, embedded in low melt agarose, and 200 µm thickness slices were cut with a LeicaVT1200S vibratome (Leica Biosystems). For dissociation assays, slices were washed gently with HBSS, transferred to pre-warmed cardiac slices medium, and incubated for 1 h with indicated mediators at 37°C, 5% CO_2.

4.3 | Mediators and reagents

HL-1 cells and murine cardiac slices were treated with mediators for 60 min. Concentrations and functions of the mediators or reagents used are listed in Table 1.

4.4 | Transmission electron microscopy

TEM in murine cardiac slice cultures was performed as described previously.[11,15] Briefly, cardiac slices were fixed with 1% glutaraldehyde in PBS for 2 h at 4°C. After washing with PBS for three times, tissue was post-fixed in 2% Osmium tetroxide, dehydrated through an ascending ethanol series subsequently embedded in EPON 812 (Serva Electrophoresis GmBH, Heidelberg, Germany) and cured at 80°C for 24 h. After trimming, ultrathin sections (60 nm) were cut with a diamond knife (DiATOME Electron Microscopy Sciences, Hatfield, USA) and placed on copper/rhodium grids (150 mesh, Plano GmbH, Wetzlar, Germany). Contrasting was performed with a saturated uranyl acetate solution and lead(II) citrate according to standard protocols (Watson, 1958; Reynolds, 1963). Images were acquired using a Libra 120 transmission electron microscope (Carl Zeiss NTS GmbH, Oberkochen, Germany) equipped with a SSCCD camera system (TRS, Olympus, Tokyo, Japan).

For quantitative analysis, 25 ICDs per mouse per condition were analyzed by a blindfolded observer using ImageJ software (NIH). Plaque thickness was determined by measuring from the lateral end of one plaque to the lateral end of the plaque of the adjacent cell and subtracting the measured intercellular space. Measurement was done three times per ICD and averaged to level out differences within one ICD. Area composita length was measured by following the convolution of each ICD and the lengths were displayed in micrometer. An area of 56 μm^2 per image was analyzed and a minimum of five images were analyzed per mouse.

4.5 | Immunostaining

Immunostaining in HL-1 cells was performed as described previously.[13] In brief, cells were seeded on coverslips and fixed with 2% paraformaldehyde (PFA) after respective treatments. Immunostaining in murine cardiac slices were performed in 7 µm thick sections cut with a cryostat (HM500OMV, Microm, Walldorf, Germany), sections were transferred to glass slides and adhered by warming up to 38°C and fixed with 2% PFA. After PFA fixation, the samples were permeabilized with 0.1% Triton-X 100 and blocked with bovine serum albumin and normal goat serum (BSA/NGS). Post-fixation cells were permeablized with 0.1% Triton-X 100, blocked with bovine serum albumin and normal goat serum (BSA/NGS), incubated with primary antibodies diluted in PBS overnight at 4°C in a wet chamber. Following primary antibodies were used: N-CAD (BD Transduction Laboratories, #610921), DSG2 (Progen,

TABLE 1 Concentration and function of mediators

Name	Function	Final concentration	Company and catalog no.
Carbachol (CCH)	Cholinergic agonist	40 µmol/L	Sigma;C4382
Forskolin	Adenylate cyclase activator	10 µmol/L	Sigma; F3917
Rolipram	Phosphodiesterase-4-Inhibitor	5 µmol/L	Sigma; R6520
Wortmannin	PI3K inhibitor	100 nmol/L	Sigma;12–338

#610121), DP (Progen, #61003), PG (Progen, #61 005) and PKP2 (Progen, #651167). When working with HL-1 cardiomyocytes, PBS was used for washing steps, while for murine tissue samples, 50 mM NH4Cl in PBS was used. Fluorophore-coupled secondary antibodies anti-mouse Alexa Fluor 488 1:100 (Dianova #115–545-003), anti-mouse Cy3 (Dianova 115–165-164), anti-rabbit Cy5 1:600 (Dianova, 111–175-144) and DAPI (Roche, #10236276001) were added for 60 min. In the case of wheat germ agglutinin (WGA), the dye was added together with the secondary antibodies. WGA was used at 2 μg/ml concentration. After washing three times 5 min each, coverslips were mounted on microscope slides using NPG (Sigma-Aldrich, #P3130). Slides were analyzed using a Leica SP5 confocal microscope (Leica, Mannheim, Germany) with a 63X oil objective and the LAS-AF software. Colocalization analyses in HL-1 cells were performed as described before,[13] in brief, the membrane was marked as a region of interest. In this region, the amount of stained pixels in the other channels was measured and a ratio of colocalization at the membrane was calculated. Fluorescence intensities of proteins in the ICDs were measured using Image J software, by drawing a region of interest in the area stained with WGA and the same region of interest was overlaid on the channel where the target protein was detected, and a mean gray value was measured for each image. Average of the control mean gray values was normalized to one and the respective treatment values were calculated.

4.6 | Dissociation assays

Dispase-based dissociation assays in HL-1 cells were performed as described before.[10,11,13,15] In brief, after the respective treatments, medium was removed and replaced by Liberase-DH (Sigma-Aldrich, #5401054001) followed by Dispase II (Sigma-Aldrich, #D4693). Cells were incubated at 37°C, 5%CO_2, until the cell monolayers detached from the well bottoms. Then, the enzyme mix was replaced by HBSS, and mechanical stress was applied by shaking at 1.31 g for 5–10 min on an orbital shaker (Stuart SSM5 orbital shaker). For better visibility, cells were incubated with MTT (Sigma-Aldrich, #M5655) for 3 min, and images were taken to count the number of fragments. The amount of fragmentation serves as an indirect measurement of intercellular cohesion, as fewer fragments suggest a stronger cellular cohesion.

Dissociation assays in murine cardiac slices were performed similarly to dissociation assays in HL-1 cells. However, in this case, Liberase-DH and Dispase II were added together for 30 min. MTT was added and mechanical stress was applied using an electrical pipette by pipetting up and down. The same mechanical stress was applied to the other slices of the same experiment. Then the content of each well was filtered using a 70 μm nylon membrane, pictures of the well were taken and stitched together using the AutoStich software. For quantification, only the number of dissociated cardiomyocytes stained with MTT were counted. To control variations due to different slice size or location in the ventricle, consecutive slices for control and treatment were used, respectively, and the result of a slice was normalized to the respective control slice.

4.7 | Atomic force microscopy

Atomic force microscopy (AFM) measurements were performed as described before[10,11] using a Nanowizard III AFM (JPK Instruments, Berlin, Germany) with an optical fluorescence microscope (Axio Observer D1, Carl Zeiss) at 37°C. AFM cantilevers (MLCT AFM Probes, Bruker, Calle Tecate, Ca, USA) were coated with recombinant DSG2-Fc as described previously.[33] For experiments, HL-1 cells which were seeded on 24 mm coverslips were measured with the D-tip of the cantilever. A bright-field image of the cells of interest was acquired with a 63x objective. After the acquisition of a topographic image (settings: retraction speed: 50 μm/s, 4 px/μm, indentation force: 0.5nN, retraction height 2500 nm) to identify cell borders. Adhesion measurements were performed on cell borders and cell surfaces on an area of 1.5 μm × 5 μm and 2 × 2 μm, respectively (indentation force: 0.5 nN, retraction height: 3 μm, retraction speed: 10 μm/s, extend and retract delay: 0.1 s). Each pixel corresponds to a force-distance curve comprising adhesion information at this position. In the case of binding events, the force required to rupture the binding is called unbinding force. Same cells were analyzed before and after 1 h of CCH treatment. The binding frequency was determined for each condition as the number of force-distance curves showing unbinding events over the total number of curves.

4.8 | Lysate preparation

For Western blot analyses, lysates were prepared in SDS lysis buffer with protease and phosphatase inhibitors (cOmplete Protease Inhibitor Cocktail, Roche, #CO-RO and PhosStop, Roche, #PHOSS-RO). In the case of HL-1 cells, the medium was removed after respective treatments, and cells were kept on ice, washed with PBS, scraped into SDS lysis buffer, and sonicated. Murine cardiac slices were treated, washed with HBSS, and snap-frozen in liquid nitrogen. To prepare the tissue lysates, SDS lysis buffer was added, the samples were transferred

into gentleMACS M-tubes (Miltenyi Biotec, #130–093-236) and dissociated using the protein_01_01 program of the gentleMACS OctoDissociator (Miltenyi Biotec, #130–095-937).

For immunoprecipitation experiments, cells were cultured in T75 flasks. After treatments, RIPA lysis buffer (10 mM Na_2HPO_4, 150 mM NaCl, 1% Triton X-100, 0.25% SDS, 1% sodium deoxycholate, pH = 7.2) containing protease and phosphatase inhibitors were added to the cells and incubated for 30 min on ice on a rocking platform. The lysate was then transferred to gentleMACS M-tubes and dissociated using the protein_01_01 program of the gentleMACS OctoDissociator.

For Triton assays, cells were washed with ice-cold PBS and kept on ice on a rocking platform in Triton buffer (0.5% Triton X-100, 50 mM MES, 25 mM EGTA, 5 mM $MgCl_2$, pH = 6.8) with protease and phosphatase inhibitors for 20 min. Then the lysates were transferred to Eppendorf tubes and centrifuged at 4°C for 10 min at 15000*g* in an Eppendorf 5430R centrifuge. Next, the supernatant containing the Triton-soluble proteins was transferred to a new reaction tube, while the pellets were washed with Triton buffer, dissolved in SDS lysis buffer, and sonicated.

For all assays, protein concentration was measured using the Pierce Protein Assay Kit (Thermo Fisher, #23225) according to the manufacturer's protocol.

4.9 | Immunoprecipitation

Immunoprecipitations were done by mixing 1.5 mg of protein lysate and 1 μg of respective antibodies overnight at 4°C on a spinning wheel. To rule out unspecific antibody or bead binding, IgG control samples were prepared in parallel. Same amount of protein lysate was used as for pulldowns. However, 1 μg of normal mouse IgG (Merck, #12–371) was added to the samples instead of the primary antibody. Further, pulldowns were performed with Protein G Dynabeads (Thermo Fisher, #10004D) by adding the lysate-antibody mix for 1 h at 4°C on a spinning wheel to beads prewashed in RIPA buffer with protease and phosphatase inhibitors. Washing steps were performed using a magnetic rack. Then, beads were washed twice with wash buffer 1 (50 mM Tris–HCl, 150 mM NaCl, 0.1 mM EDTA, 0.5% Tween20, pH = 7.5), thrice with wash buffer 2 (100 mM Tris–HCl, 200 mM NaCl, 2 M Urea, 0.5% Tween20, pH = 7.5), and twice with 1% Triton X-100 in PBS. All wash buffers were supplemented with protease and phosphatase inhibitors. After the last wash step, beads were resuspended in Laemmli buffer, denatured for 10 min at 95°C; the lysate was separated from the beads using a magnet and loaded on a SDS–PAGE gel for Western blot analyses: 20 μg of total lysate was used as input control for the Western blots.

4.10 | Western blot analyses

Lysates were denatured in Laemmli buffer and boiled for 10 min at 95°C, before being loaded on SDS–PAGE gels. The PageRuler Plus Prestained Protein Ladder (Thermo Fisher, #26620) was used as a marker. After electrophoresis, proteins were transferred to a nitrocellulose membrane (Thermo Fisher, #LC2006) using the wet-blot method. Membranes were then blocked in 5% milk/TBST, in case of anti-phospho-EGFR antibodies in 5% BSA/TBST, or in case of anti-DP antibodies in ROTI Block (Carl Roth, #A151.2). Following primary antibodies were added overnight at 4°C on a rocking platform: anti-AKT (Cell signaling #9272), anti-phospho-AKT (serine 473, Cell signaling #4060), anti-DP (Progen, #61003), anti-phospho-ERK1/2 ([E-4] Santa Cruz, #sc-7383), anti-ERK (Cell Signaling, #9102), anti-GSK-3β (3D10) (Cell signaling #9832), anti-Phospho-GSK-3β (serine 9, Cell signaling #5558), anti-phospho-PG (serine 665, self-made as described before[15]), anti-PG ([PG5.1] Progen #61005), anti-PKP2 (Progen, #651167), and anti-α-tubulin ([DM1A], abcam, #ab7291). After washing, membranes were incubated with species-matched, HRP-coupled secondary antibodies (Dianova, #111–035-045 or #115–035-068) diluted in TBST or 5% milk/TBST in case of phospho-EGFR antibodies, and developed using an iBright FL1500 (Thermo Fisher) developer with SuperSignal West Pico PLUS Chemiluminescent Substrate (Thermo Fisher, #34577). All primary antibodies were used at 1:1000 dilutions, apart from phospho-PG (1:20), anti-PKP2 (1:25) and anti-α-tubulin (1:4000). Quantification was performed using the Image Studio Lite v.5.2 or the iBright Analysis Software (Invitrogen).

4.11 | siRNA-mediated knockdown

For siRNA-mediated knockdown, cells were transfected with a transfection reagent comprised of OptiMEM (Thermo Scientific, #31985070), RNAiMAX (Thermo Scientific #13778150), and the ON-Target siRNA (Dharmacon, siNT #D-001810-10, siDsg2 #L-042514-01, siDp #L-040653-01, siPg#L-040316-01, and siPkp2#L-040672-01) according to manufacturer's protocol. Cells were transfected for 24 h, and medium was changed, followed by another medium change 48 h post-transfection. Experiments were performed 72 h post-transfection. Each knockdown was confirmed by Western blot.

4.12 | Imaging and statistics

Images were processed with Adobe Photoshop CC19, Image Studio Lite v.5.2 and ImageJ software. Statistical analyses were performed using GraphPad Prism 9 and are explained in figure legends. Data are represented as mean ± standard error of the mean (SEM). For dissociation assays in HL-1 cells and Western blot quantification data, values were normalized to the average control value of all experiments. In addition, the number of dissociated cells was normalized to the respective control slice of the same mouse for dissociation assays with murine cardiac slices. Significance was assumed for $p \leq 0.05$.

ACKNOWLEDGMENTS

We thank Kathleen Plietz and Kilian Skowranek for their technical assistance. Open Access funding enabled and organized by Projekt DEAL.

FUNDING INFORMATION

This work was supported by the Ludwig-Maximilian-University Munich through the FöFoLe program (to LK), Fredrich-Baur-stifftung (Reg.-Nr. 01/19 to SY), and the Deutsche Forschungsgemeinschaft (grant WA2474/11–1 to JW).

CONFLICT OF INTEREST

The authors declare no conflict of interest.

ORCID

Sunil Yeruva https://orcid.org/0000-0002-1565-2023
Jens Waschke https://orcid.org/0000-0003-1182-5422

REFERENCES

1. Goldberger JJ, Arora R, Buckley U, Shivkumar K. Autonomic nervous system dysfunction: JACC focus seminar. *J Am Coll Cardiol*. 2019;73(10):1189-1206.
2. Chatterjee NA, Singh JP. Autonomic modulation and cardiac arrhythmias: old insights and novel strategies. *Europace*. 2021;23(11):1708-1721.
3. Hadaya J, Ardell JL. Autonomic modulation for cardiovascular disease. *Front Physiol*. 2020;11:617459.
4. Caulfield MP. Muscarinic receptors--characterization, coupling and function. *Pharmacol Ther*. 1993;58(3):319-379.
5. Dhein S, van Koppen CJ, Brodde OE. Muscarinic receptors in the mammalian heart. *Pharmacol Res*. 2001;44(3):161-182.
6. Wang Z, Shi H, Wang H. Functional M3 muscarinic acetylcholine receptors in mammalian hearts. *Br J Pharmacol*. 2004;142(3):395-408.
7. Rampazzo A, Calore M, van Hengel J, van Roy F. Intercalated discs and arrhythmogenic cardiomyopathy. *Circ Cardiovasc Genet*. 2014;7(6):930-940.
8. Delmar M, McKenna WJ. The cardiac desmosome and arrhythmogenic cardiomyopathies: from gene to disease. *Circ Res*. 2010;107(6):700-714.
9. Schlipp A, Schinner C, Spindler V, et al. Desmoglein-2 interaction is crucial for cardiomyocyte cohesion and function. *Cardiovasc Res*. 2014;104(2):245-257.
10. Schinner C, Vielmuth F, Rotzer V, et al. Adrenergic signaling strengthens cardiac myocyte cohesion. *Circ Res*. 2017;120(8):1305-1317.
11. Schinner C, Olivares-Florez S, Schlipp A, et al. The inotropic agent digitoxin strengthens desmosomal adhesion in cardiac myocytes in an ERK1/2-dependent manner. *Basic Res Cardiol*. 2020;115(4):46.
12. Claycomb WC, Lanson NA Jr, Stallworth BS, et al. HL-1 cells: a cardiac muscle cell line that contracts and retains phenotypic characteristics of the adult cardiomyocyte. *Proc Natl Acad Sci U S A*. 1998;95(6):2979-2984.
13. Shoykhet M, Trenz S, Kempf E, et al. Cardiomyocyte adhesion and hyperadhesion differentially require ERK1/2 and plakoglobin. *JCI Insight*. 2020;5(18):e140066.
14. Fuchs M, Kugelmann D, Schlegel N, Vielmuth F, Waschke J. Desmoglein 2 can undergo Ca(2+)-dependent interactions with both desmosomal and classical cadherins including E-cadherin and N-cadherin. *Biophys J*. 2022;121:1322-1335.
15. Yeruva S, Kempf E, Egu DT, Flaswinkel H, Kugelmann D, Waschke J. Adrenergic signaling-induced ultrastructural strengthening of intercalated discs via plakoglobin is crucial for positive adhesiotropy in murine cardiomyocytes. *Front Physiol*. 2020;11:430.
16. Baine S, Thomas J, Bonilla I, et al. Muscarinic-dependent phosphorylation of the cardiac ryanodine receptor by protein kinase G is mediated by PI3K-AKT-nNOS signaling. *J Biol Chem*. 2020;295(33):11720-11728.
17. Zhou L, Jiang ZM, Qiu XM, Zhang YK, Zhang FX, Wang YX. Carbachol alleviates myocardial injury in septic rats through PI3K/AKT signaling pathway. *Eur Rev Med Pharmacol Sci*. 2020;24(10):5650-5658.
18. Albrecht LV, Zhang L, Shabanowitz J, et al. GSK3- and PRMT-1-dependent modifications of desmoplakin control desmoplakin-cytoskeleton dynamics. *J Cell Biol*. 2015;208(5):597-612.
19. Fukuda K, Kanazawa H, Aizawa Y, Ardell JL, Shivkumar K. Cardiac innervation and sudden cardiac death. *Circ Res*. 2015;116(12):2005-2019.
20. Vaseghi M, Shivkumar K. The role of the autonomic nervous system in sudden cardiac death. *Prog Cardiovasc Dis*. 2008;50(6):404-419.
21. Yeruva SP, Waschke J. Structure and regulation of desmosomes in intercalated discs: lessons from epithelia. *J Anat*. 2022. doi: 10.1111/joa.13634 [Online ahead of print]
22. Grando SA. Cholinergic control of epidermal cohesion. *Exp Dermatol*. 2006;15(4):265-282.
23. Nguyen VT, Arredondo J, Chernyavsky AI, Kitajima Y, Grando SA. Keratinocyte acetylcholine receptors regulate cell adhesion. *Life Sci*. 2003;72(18–19):2081-2085.
24. Spindler V, Waschke J. Pemphigus-a disease of desmosome dysfunction caused by multiple mechanisms. *Front Immunol*. 2018;9:136.
25. Grando SA, Pittelkow MR, Schallreuter KU. Adrenergic and cholinergic control in the biology of epidermis: physiological and clinical significance. *J Invest Dermatol*. 2006;126(9):1948-1965.
26. Ho HT, Belevych AE, Liu B, et al. Muscarinic stimulation facilitates sarcoplasmic reticulum ca release by modulating

ryanodine receptor 2 phosphorylation through protein kinase G and ca/calmodulin-dependent protein kinase II. *Hypertension*. 2016;68(5):1171-1178.
27. De Sarno P, Bijur GN, Zmijewska AA, Li X, Jope RS. In vivo regulation of GSK3 phosphorylation by cholinergic and NMDA receptors. *Neurobiol Aging*. 2006;27(3):413-422.
28. Mans RA, Hinton KD, Payne CH, Powers GE, Scheuermann NL, Saint-Jean M. Cholinergic stimulation of the adult zebrafish brain induces phosphorylation of glycogen synthase kinase-3 beta and extracellular signal-regulated kinase in the telencephalon. *Front Mol Neurosci*. 2019;12:91.
29. Espada S, Rojo AI, Salinas M, Cuadrado A. The muscarinic M1 receptor activates Nrf2 through a signaling cascade that involves protein kinase C and inhibition of GSK-3beta: connecting neurotransmission with neuroprotection. *J Neurochem*. 2009;110(3):1107-1119.
30. Wallukat G, Fu HM, Matsui S, Hjalmarson A, Fu ML. Autoantibodies against M2 muscarinic receptors in patients with cardiomyopathy display non-desensitized agonist-like effects. *Life Sci*. 1999;64(6–7):465-469.
31. Fu ML. Anti-M2 muscarinic receptor autoantibodies and idiopathic dilated cardiomyopathy. *Int J Cardiol*. 1996;54(2):127-135.
32. Yoshizawa A, Nagai S, Baba Y, et al. Autoimmunity against M(2)muscarinic acetylcholine receptor induces myocarditis and leads to a dilated cardiomyopathy-like phenotype. *Eur J Immunol*. 2012;42(5):1152-1163.
33. Hiermaier M, Kliewe F, Schinner C, et al. The Actin-binding protein alpha-adducin modulates desmosomal turnover and plasticity. *J Invest Dermatol*. 2021;141(5):1219-1229 e1211.

SUPPORTING INFORMATION

Additional supporting information can be found online in the Supporting Information section at the end of this article.

How to cite this article: Yeruva S, Körber L, Hiermaier M, Egu DT, Kempf E, Waschke J. Cholinergic signaling impairs cardiomyocyte cohesion. *Acta Physiol*. 2022;236:e13881. doi: 10.1111/apha.13881